

Karman constant and accurate mean flow prediction in a turbulent pipe

Authors: Zhen-Su She*¹, Xi Chen¹, You Wu¹, Fazle Hussain^{1,2}

Affiliations:

¹*State Key Laboratory for Turbulence and Complex Systems and Department of Mechanics, College of Engineering, Peking University, Beijing, 100871, China*

²*Department of Mechanical Engineering, University of Houston, Houston, TX, 77204-4006, USA*

* *Email address: she@pku.edu.cn*

1 **Summary**

2 The Karman constant κ - widely used in atmospheric science and engineering
3 turbulence modelling, and proposed by Prandtl¹ in 1925 and von Karman² in 1930 to
4 describe the mean velocity of a turbulent wall-bounded flow³ - leads to a logarithmic
5 profile in an overlap region near the wall. For over eighty years, its value was believed
6 to be ~ 0.41 . But more recently, many argue that it is not a constant, because of
7 measured variations in different flows and at different Reynolds numbers $(Re)^{4-6}$. Here,
8 a multi-layer analytic theory⁷ is shown to lead to a re-interpretation of κ as a global
9 constant for both the overlap region and outer flow, and to yield a new method for its
10 measurement. The newly determined value is 0.45 for both channel and pipe. It is
11 shown that this new κ , together with other wall constants, yields a 99% accuracy in the
12 prediction of mean velocity data at *all points* in high Re (up to 40 million) pipe flow.
13 The theory also describes finite Re effect, and discovers a transition at the friction Re
14 (i.e. Re_τ) = 5000. An accurate model for the prediction of turbulent transport in
15 canonical pipe and channel flows is achieved here, and we propose the model to be
16 valid for a wide class of turbulent flows.

17

18 **Text**

19 Accurate prediction of turbulent flow remains a top challenge in classical physics.
20 Even for simple wall-bounded flows such as pipe and channel, analytic prediction of
21 mean velocities at very high Re relies on empirical functions⁸ with compromised
22 accuracy, and continues to receive vivid attention with great experimental efforts⁹⁻¹⁴.
23 Deriving a mean-field prediction based on first principles is highly desired, as it would
24 reveal new statistical symmetries governing turbulent fluctuations and allow a deeper
25 understanding of important constants describing the flow.

26 Prandtl¹ in 1925, and von Karman² in 1930, independently suggested the concept of
27 *mixing length* - analogous to the mean free path for molecular collisions - to model
28 turbulent transport. A simple model of the mixing length with linear dependence on the
29 distance from the wall yields a logarithmic mean velocity profile (MVP), where a
30 proportionality constant - the Karman constant κ - was introduced. However, this
31 empirical model has led to controversies: Barenblatt and co-authors¹⁵⁻¹⁶ have claimed
32 that power-law is a better description. Indeed, theoretical interpretation of the log-law is
33 very unsatisfactory. For example, very little is understood about κ and the other log-law
34 constant B ; their variability with different flows and different Re remains elusive⁴⁻⁶.
35 While the log-law vs. power law debate is still vivid¹⁷⁻¹⁸, we present a coveted theory
36 which re-interprets κ with a new method for its measurement. Not only a more
37 accurate description of the entire MVP over a wide range of Re is obtained, the theory
38 also predicts, for the first time, a critical Re in Princeton pipe experiment, and derives
39 quantities of engineering interest. The theory presented here provides a general guide

40 for accurate mean-field prediction from post-analysis of massive simulation data for a
41 wide class of turbulent flows.

42 The mean velocity in a turbulent pipe flow has resisted analytic attack since the turn
43 of the last century⁹. We overcome this bottleneck by developing a symmetry analysis on
44 the mean momentum equation (MME), utilizing empirical knowledge about the
45 multiple layers. For a channel or a pipe, the MME has an exact first-integral¹⁹, written
46 in wall units as

$$47 \quad S^+ + W^+ = 1 - y^+ / \text{Re}_\tau = r, \quad (1)$$

48 where $S^+ = dU^+ / dy^+$ is the mean shear and $W^+ = -\langle u'v' \rangle^+$ is the Reynolds stress,
49 and y^+ the distance to the wall, r the distance to the center, Re_τ the friction Reynolds
50 number, and $+$ denotes normalization using wall units. Our symmetry analysis involves
51 a length determined by the two primary variables, W^+ and S^+ , which is, by
52 dimensional argument, $\ell_M^+ = \sqrt{W^+} / S^+$. This length is regarded⁷ as an “order
53 parameter” used to represent effects of fluctuations in statistical mean-field theory²⁰,
54 and happens to coincide with the mixing length^{1,2} for describing the vertical mean
55 momentum transport. The concept of length order parameter is more general, however,
56 and is applicable to analyze other flows.

57 The symmetry analysis of the multi-layer structure is accomplished by a Lie-group
58 theory⁷ which derives the entire profile of the mixing length in two steps: First, identify
59 local invariant solutions for each of the layers: well known as sublayer, buffer layer,
60 bulk zone, and a new central zone called ‘core’. Each of the layers is postulated to
61 possess a local scaling for the mixing length or its gradient under the dilation

62 transformation. Then, the theory⁷ postulates a transition ansatz and derives a combined,
 63 analytic expression for the entire profile of the mixing length:

$$64 \quad \ell_M^+ = \rho \left(\frac{y^+}{y_{sub}^+} \right)^{3/2} \left(1 + \left(\frac{y^+}{y_{sub}^+} \right)^{p_I} \right)^{1/(2p_I)} \left(1 + \left(\frac{y^+}{y_{buf}^+} \right)^{p_{II}} \right)^{-1/p_{II}} \frac{1-r^m}{m(1-r)Z_{core}} \left(1 + \left(\frac{r}{r_{core}} \right)^{-p_{IV}} \right)^{1/(2p_{IV})}. \quad (2)$$

65 This determines the mean shear profile¹⁹

$$66 \quad S^+ = (-1 + \sqrt{4r\ell_M^{+2} + 1}) / (2\ell_M^{+2}), \quad (3)$$

67 hence the mean velocity profile $U^+ = \int S^+ dy^+$, the average velocities

$$68 \quad (\overline{U^+}^{Pipe} = 2 \int U^+ r dr \text{ and } \overline{U^+}^{CH} = \int U^+ dr), \text{ and the friction factor } C_f = 8 / \overline{U^+}^2. \text{ While}$$

69 previous work reported heuristic and systematic derivation⁷ of Eq.(2), the main task
 70 here is to determine the parameters with a systematic method, and to demonstrate that
 71 the Karman constant is indeed a constant, and that there is a transition at $Re_\tau = 5000$.

72 Two sets of parameters appear in Eq.(2). The *first* are four coefficients:

73 $\rho, y_{sub}^+, y_{buf}^+, r_{core}$; the *second* are called transition sharpnesses: p_I, p_{II}, p_{IV} , which
 74 describe the transition between sublayer and buffer, buffer and log region, and bulk and
 75 core. The second set, less sensitive to the predictions, are chosen to be integers
 76 ($p_I = p_{II} = 4, p_{IV} = 2$). We focus below on the determination of the four coefficients.

77 First, the inner solution near the wall determines ρ and y_{sub}^+ . From Eq.(2), we

78 find that for $y^+ \ll y_{sub}^+, \ell_M^+ \approx \rho (y^+ / y_{sub}^+)^{3/2}$. If the local scaling exists,

79 $\ell_M^+ / y^{+3/2} \approx \rho (y_{sub}^+)^{-3/2}$ is a constant near the wall, determined by ρ and y_{sub}^+ . Fig.1

80 shows that well resolved direct numerical simulation (DNS) data for channel flow
 81 indeed confirms the existence of the constant, with a value of 0.0315. In order to

82 determine y_{sub}^+ , note that it is the location where the local scaling is in the middle of 3/2
83 (sublayer scaling) and 2 (buffer scaling); thus, $d \ln \ell_M^+ / d \ln y^+ |_{y_{sub}^+} = (1+3/2)/2 = 7/4$.
84 Furthermore, we assume, with accurate empirical support from DNS data, that this
85 transition point coincides with the maximum of $\Gamma = S^+ y^+$, the diagnostic function used
86 to quantify near-wall statistics⁴. With the assumption $d\Gamma(y_{sub}^+)/dy^+ = 0$, we
87 differentiate Eq.(1) at $y^+ = y_{sub}^+$ to derive the following appealing results:
88 $S^+(y_{sub}^+) = 3/5$, $W^+(y_{sub}^+) = 2/5$, $\ell_M^+(y_{sub}^+) = \sqrt{10}/3$. This yields the prediction:
89 $\rho_0 \approx 2^{3/8} \sqrt{5}/3 \approx 0.967$; then, using the above empirical near-wall measurement, we
90 obtain $y_{sub}^+ \approx 9.80$.

91 Next, Eq.(2) predicts an analytic scaling function for the mean defect velocity (i.e.
92 difference from the centreline velocity U_c^+) (see Fig.2). Fig.2a confirms this linear
93 relation for channel (DNS) and pipe (Princeton data) over a wide range of Re (a
94 complete collapse); then, κ is derived from the slope with high accuracy. Fig.2b
95 shows a procedure for the determination of r_{core} . A conservative estimate of the
96 Karman constant is $\kappa \approx 0.45 \pm 0.014$; the measured r_{core} for Princeton pipe data is
97 $r_{core}^{(\infty)} \approx 0.67 \pm 0.3$, which is believed to be the asymptotic value at high Re . From the
98 matching condition, $\kappa = \rho y_{buf}^+ / y_{sub}^{+2}$, we obtain $y_{buf}^{+(\infty)} \approx 44.7$. Fig. 3 compares our
99 predicted MVP with Princeton pipe data using these four parameter values, showing
100 uniform agreement of the entire profile with 99% accuracy for Re up to forty million.
101 This unprecedented accuracy, based on objectively measured physical parameters,
102 supports that turbulence in pipe indeed admits an analytic solution!

103 Note, however, that the core-layer thickness for DNS channel data at moderate Re
104 (Fig.2b) shows notable difference from Princeton pipe data: $r_{core}^{DNS} \approx 0.27$. We attribute
105 it to finite Re effect which can now be studied. Define $r_{core}^{DNS} \approx r_{core}^{(\infty)}(1 - \varepsilon_c)$, then
106 departure at DNS Re ($Re_\tau \approx 10^3$) gives $\varepsilon_c \approx 0.6$. Furthermore, we believe that the
107 Re -effect in the bulk flow (r_{core}) would influence the overlap region (y_{buf}^+), leading to a
108 change in $\rho = \rho_0(1 + \varepsilon_\rho)$. Fig.1(b) indeed shows evidence of such departure with
109 $\varepsilon_\rho \approx 0.1$, which yields a higher plateau of 0.035. The Re -effect is further validated by
110 the measured centreline velocity U_c^+ and average velocity \overline{U}^+ , and skin friction
111 coefficient C_f derived from Eq.(2) (see the Method). Fig.3b, using a compensated
112 plot against asymptotic high Re result, shows clearly that a transition takes place around
113 $Re_\tau^{(crit)} \approx 5000$. Furthermore, a simple model for linear dependence of ε_ρ and ε_c on
114 Re below $Re_\tau^{(crit)}$ yields an accurate description of friction coefficients for all pipe data.

115 The theory also derives several empirical constants of engineering interest. A
116 Re -independent quantity for pipe can be predicted: $(U_c^+ - \overline{U}^+)^{Pipe} \approx 4.3$, which is very
117 close to the empirical value (see Fig.3b), improving Pope's derivation³, i.e. $1.5/\kappa$ (3.3,
118 using $\kappa \approx 0.45$). Furthermore, we derive a new formula for turbulent pipe for a widely
119 useful relation between Re_τ and Re : our result, $Re_\tau \approx 0.26 Re / \ln Re$, should replace
120 the popular empirical formula³: $Re_\tau \approx 0.09 Re^{0.88}$. The latter has an error of up to 25%
121 at $Re_\tau = 5 \times 10^5$ according to Princeton data; ours is less than 1%. We also predict a

122 constant difference of centreline velocity between channel and pipe:

123 $U_c^{+Pipe} - U_c^{+CH} \approx 1.1$, in sharp contrast to [19] which predicts a notable Re -dependence.

124 In summary, we have achieved an accurate description of turbulent mean velocity,

125 which differentiates the effect of geometry (pipe versus channel) with a single integer

126 ($m=5$ versus $m=4$), and identified four physical parameters which are *not* fitting

127 parameters, but measured systematically from accurate experimental/numerical data.

128 We obtain also the first theory which predicts finite Re effect, and discovers a transition

129 at $Re_\tau^{(crit)} \approx 5000$ for the friction factor. The most notable outcome is the universality of

130 κ ; it resets the status of the Karman constant to be intimately related to universal

131 small-scale dynamics of fully developed bulk flow turbulence, even possibly to the

132 Kolmogorov constant²⁴.

133 The conceptual framework developed here is encompassing and goes far beyond

134 the classical mixing length theory, as the mixing length is used here to reveal the

135 *complete* multi-layer structure which is a general feature of a wide class of

136 wall-bounded turbulent flows. We also show a procedure for extracting quantitative

137 information from empirical data, which can be adapted to a variety of turbulent flows.

138 Indeed, the analysis has been successfully extended to incompressible, compressible

139 and rough-wall turbulent boundary layers, and our results will soon be communicated.

140 Another interesting application underway is turbulent Rayleigh-Benard convection²⁵;

141 the mean profiles (of velocity and temperature) can now be quantitatively described by

142 a symmetry study of the mixing length and one or more order functions associated with

143 temperature fluctuations.

144

145 **Method**

146 Analytic expressions for mean velocities can be derived from Eq.(2), to yield a
 147 systematic procedure for determining four physical model parameters. In the outer
 148 region, Eq.(1) yields: $dU^+ / dr \approx -\sqrt{r} / \ell_M$. Then, using Eq.(2) for $y^+ \gg y_{buf}^+$:

149
$$U^{+(Outer)}(r) = U^+(0) - \frac{1}{\kappa} f(r, r_{core}) = U_c^+ - \frac{m}{\kappa} Z_{core} \int_0^r \frac{r' dr'}{(1-r'^m)(r'^2+r_{core}^2)^{1/4}}, \quad (4)$$

150 where $f(r, r_{core})$ characterizes the bulk mean flow and depends only on one parameter:
 151 r_{core} . Once r_{core} is specified, it is a simple least-squares problem to derive optimal
 152 values of κ and U_c^+ from a set of measured mean velocities, $U^{+EXP}(r_i)$. The
 153 determination of r_{core} is realized using the relative error function,

154
$$\sigma_U = \frac{1}{N} \sum (1 - U^+(r_i) / U^{+EXP}(r_i))^2$$
, which measures how close the function $f(r, r_{core})$

155 describes the real data $U^{+EXP}(r_i)$. Note r_{core} and κ are determined by independent
 156 criteria. The validity of the method is clearly demonstrated in Fig.2.

157 Analysis of empirical data shows that both r_{core} and ρ have notable
 158 Re -dependence, while κ and y_{sub}^+ are remarkably universal. To further elaborate on
 159 this, analytic expression for the centreline velocity is derived below. Let us write:

160
$$U_c^+(Re_\tau) = U_{buf}^+ + \Delta U_{bulk}^+ + \Delta U_{core}^+ \approx \int_0^{y_{buf}^+} \frac{-1 + \sqrt{4\ell_M^{+2} + 1}}{2\ell_M^{+2}} dy^+ + \left(\int_{y_{buf}^+}^{y_{core}^+} + \int_{y_{core}^+}^{Re_\tau} \right) \frac{\sqrt{r}}{\ell_M^+} dy^+, \quad (5)$$

161 where the near-wall contribution is expressed by $U_{buf}^+ = U^+(y_{buf}^+)$, the bulk by ΔU_{bulk}^+ ,
 162 and the core layer by ΔU_{core}^+ , with $y_{core}^+ = (1 - r_{core}) Re_\tau$. Finite Re effect is described by
 163 two small parameters, ε_ρ and ε_c , defined as $\rho = \rho_0(1 + \varepsilon_\rho)$ (hence

164 $y_{buf}^+ = y_{buf}^{+(\infty)}(1 - \varepsilon_\rho)$ and $r_{core} = r_{core}^{(\infty)}(1 - \varepsilon_c)$. A perturbation analysis yields:

165 $U_{buf}^+(\varepsilon_\rho) \approx y_{buf}^{+(\infty)}(0.33 - 0.20\varepsilon_\rho)$. Substitute $\ell_M^{(bulk)} \approx \kappa(1 - r^m)/m$ into (6), to obtain

166 $\Delta U_{bulk}^+ \approx [\ln(y_{core}^+ / y_{buf}^+) + \Lambda(r_{core})] / \kappa$, where $\Lambda(r) = \psi(r_{buf}) - \psi(r)$ ($r_{buf} = 1 - y_{buf}^+ / \text{Re}_\tau \approx 1$

167 for high Re) and $\psi(r)$ has an analytic expression [26]. Next, substitute

168 $\ell_M^{(core)} \approx \kappa(1 + (r_{core}/r)^2)^{1/4} / (5Z_{core})$ into (6), to obtain $\Delta U_{core}^+ \approx 5Z_{core} r_{core}^{3/2} / (2\kappa)$. Summarizing

169 all the terms above, we obtain a first-order approximation for the centreline velocity:

$$170 \quad U_c^{+Pipe(CH)} \approx U_c^{+Pipe(CH)(\infty)} - 6.72\varepsilon_\rho + 1.51(1.68)\varepsilon_c \quad (6)$$

171 where $U_c^{+Pipe(CH)(\infty)} \approx \ln(\text{Re}_\tau) / \kappa + 8.37(7.28)$. This yields, for the first time, the centreline

172 velocity difference between a pipe and a channel at the same Re :

173 $U_c^{+Pipe} - U_c^{+CH} \approx 1.09 - 0.17\varepsilon_c$. Finally, the average velocities also have an analytic

174 expression:

$$175 \quad \overline{U}^{+Pipe(CH)} \approx \overline{U}^{+Pipe(CH)(\infty)} - 6.84\varepsilon_\rho + 0.26(0.36)\varepsilon_c. \quad (7)$$

176 where $\overline{U}^{+Pipe(CH)(\infty)} \approx \ln(\text{Re}_\tau) / \kappa + 4.1(5.0)$. This allows an evaluation of the bulk velocity

177 Reynolds number in pipe: $\text{Re} = \overline{2U} / \nu = 2\overline{U}^+ \text{Re}_\tau$, and friction coefficient:

$$178 \quad C_f^{Pipe} = 8 \left(\overline{U}^{+Pipe} \right)^{-2} \approx C_f^{Pipe(\infty)} [1 + (13.68\varepsilon_\rho - 0.52\varepsilon_c) \sqrt{C_f^{Pipe(\infty)} / 8}]. \quad (8)$$

179 where $C_f^{Pipe(\infty)} = 8 \left(\overline{U}^{+Pipe(\infty)} \right)^{-2}$. A simple linear model for $\varepsilon_{\rho(c)}$ is introduced as:

$$180 \quad \varepsilon_{\rho(c)} = \varepsilon_{\rho(c)}^{(0)} (\text{Re}_\tau^{(crit)} - \text{Re}_\tau) / (\text{Re}_\tau^{(crit)} - 1000), \quad (9)$$

181 where $\varepsilon_\rho^{(0)} \approx 0.1$ and $\varepsilon_c^{(0)} \approx 0.6$ are derived from empirical data.

182

183 **References**

- 184 1. Prandtl, On fluid motions with very small friction (in German). *Third International*
185 *Mathematical Congress*. Heidelberg, 484–491 (1904).
- 186 2. von Karman, T. Mechanische Ahnlichkeit und Turbulenz. In *Proc. Third Int. Congr.*
187 *Applied Mechanics*, Stockholm. 85-105 (1930).
- 188 3. Pope, S.B. *Turbulent flows*. 264-295 (Cambridge University Press, 2000).
- 189 4. Smits A. J., McKeon B. J., Marusic I., High Reynolds number wall turbulence.
190 *Annu. Rev. Fluid Mech.* 43:353-75 (2011).
- 191 5. Nagib, H.M. and Chauhan, K.A. Variations of von Kármán coefficient in canonical
192 flows. *Phys. Fluids*. **20**, 101518 (2008).
- 193 6. Marusic, I., *et al.* Wall-bounded turbulent flows at high Reynolds numbers: Recent
194 advances and key issues. *Phys. Fluids*. **22**, 065103 (2010).
- 195 7. She, Z.S., Chen, X., Wu, Y. and Hussain, F. New perspectives in statistical
196 modeling of wall-bounded turbulence. *Acta Mechanica Sinica*. **26**, 847-861 (2010);
197 She, Z.S., Chen, X. and Hussain, F. A Lie-group derivation of a multi-layer mixing
198 length formula for turbulent channel and pipe flows, arXiv:1112.6312 (2011).
- 199 8. Wilcox, D.C. *Turbulence Modeling for CFD*. (DCW Industries, 2006), 181-182.
- 200 9. Reynolds, O. An experimental investigation of the circumstances which determine
201 whether the motion of water shall be direct or sinuous, and the law of resistance in
202 parallel channels. *Phil. Trans. R. Soc. London, Ser. A*. **174**, 935-982 (1883).
- 203 10. Zagarola, M.V. and Smits, A.J. Scaling of the mean velocity profile for turbulent
204 pipe flow. *Phys. Rev. Lett.* **78**, 239-242 (1997).

- 205 11. Swanson, C., Julian B., Ihas, G.G. and Donnelly, R., Pipe flow measurements over a
206 wide range of Reynolds numbers using liquid helium and various gases, *J. Fluid*
207 *Mech.* **461**, 51-60 (2002).
- 208 12. Zanoun, E.S., Durst, F. and Nagib, H. Evaluating the law of the wall in
209 two-dimensional fully developed turbulent channel flows. *Phys. Fluids.* **15**,
210 3079-3089 (2003).
- 211 13. B. J. McKeon, J. Li, W. Jiang, J. F. Morrison, and A. J. Smits. *J. Fluid Mech.* **501**,
212 135 (2004); the data are available at [http://gasdyn.princeton.edu/data/e248/mckeon_](http://gasdyn.princeton.edu/data/e248/mckeon_data.html)
213 [data.html](http://gasdyn.princeton.edu/data/e248/mckeon_data.html).
- 214 14. Talamelli, A. *et al.* CICLoPE—a response to the need for high Reynolds number
215 experiments. *Fluid Dyn. Res.* **41**, 021407 (2009).
- 216 15. Barenblatt, G.I. Scaling laws for fully developed turbulent shear flows. Part 1. Basic
217 hypotheses and analysis. *J. Fluid Mech.* **248**, 521-529 (1993).
- 218 16. Barenblatt, G.I., Chorin, A.J. and Prostokishin V.M. Scaling laws for fully
219 developed turbulent flow in pipes: Discussion of experimental data. *Proc. Natl.*
220 *Acad. Sci.* **94**, 773-776 (1997).
- 221 17. Zagarola, M.V., Perry, A.E. and Smits, A.J. Log laws or power laws: The scaling in
222 the overlap region. *Phys. Fluids.* **9**, 2094-2100 (1997).
- 223 18. George, W.K. Is there a universal log-law for turbulent wall-bounded flow? *Phil.*
224 *Trans. R. Soc. London, Ser. A.* **365**, 789-806 (2007).
- 225 19. L'vov, V.S., Procaccia, I. and Rudenko, O. Universal model of finite Reynolds
226 number turbulent flow in channels and pipes. *Phys. Rev. Lett.* **100**, 050504 (2008).
- 227 20. Kadanoff, L. P. More is the same; phase transitions and mean field theories. *J. Stat.*
228 *Phys.* **137**, 777–797 (2009).

- 229 21. Iwamoto, K., Suzuki, Y. and Kasagi, N. Database of fully developed channel flow.
 230 *THTLAB Internal Report*. No. ILR-0201 (2002).
- 231 22. Hoyas, S. and Jimenez, J. Scaling of the velocity fluctuations in turbulent channels
 232 up to $Re_{\tau} = 2003$. *Phys. Fluids*. **18**, 011702 (2006).
- 233 23. Wu, X.H. and Moin, P. A direct numerical simulation study on the mean velocity
 234 characteristics in turbulent pipe flow. *J. Fluid Mech.* **608**, 81-112 (2008).
- 235 24. Lo, T.S., L'vov, V.S., Pomyalov A. and Procaccia, I. Estimating von-Karman's
 236 constant from homogeneous turbulence. *Europhys. Lett.* **72**, 943 (2005).
- 237 25. Ahlers, G., Grossmann, S. and Lohse, D. Heat transfer and large scale dynamics in
 238 turbulent Rayleigh-Bénard convection. *Rev. Mod. Phys.* **81**, 503–537 (2009).
- 239 26. For pipe flow ($m=5$), the explicit form is

240
$$\psi^{Pipe}(r) = 2\ln(1+\sqrt{r}) + \frac{\sqrt{5}-1}{4}\ln\varphi^+(r) + \frac{\sqrt{5}+1}{4}\ln\varphi^-(r) + \frac{2\sqrt{5}}{c^-}\arctan\frac{c^-\sqrt{r}}{A^-(r)} - \frac{2\sqrt{5}}{c^+}\arctan\frac{c^+\sqrt{r}}{A^-(r)},$$
 where

241
$$\varphi^+(r) = \frac{A^+(r)-B^+(r)}{A^+(r)+B^+(r)}, \quad \varphi^-(r) = \frac{A^+(r)-B^-(r)}{A^+(r)+B^-(r)}, \quad A^+(r) = 2(1+r); \quad A^-(r) = 2(1-r);$$

242
$$B^+(r) = (\sqrt{5}+1)r; \quad B^-(r) = (\sqrt{5}-1)r; \quad c^+ = \sqrt{10+2\sqrt{5}}; \quad c^- = \sqrt{10-2\sqrt{5}}.$$

243

244 End Notes

245

246 **Acknowledgements** We thank G. Ahlers, E. Bodenschatch, N. Goldenfeld, H.
 247 Swinney for helpful discussions. This work was supported by the National Natural
 248 Science Foundation of China (90716008 and 10921202), MOST 973 Project
 249 (2009CB724100). Part of the work was completed during our visit at KITP of UCSB
 250 during “Turbulence program”, supported by the National Science Foundation of US

251 under Grant No. NSF PHY05-51164, which is gratefully acknowledged.

252

253 **Author Contribution**

254 Z.S.S. established the theoretical framework, and directed the research in collaboration
255 with F.H., X.C. and Z.S.S. developed the analysis, and X.C. measured the physical
256 constants. Y.W. performed quantitative study of the model and compared the
257 predictions with the empirical data. Z.S.S., X.C. and F.H. wrote the manuscript. All
258 authors extensively discussed the results and interpretations, and commented on the
259 manuscript.

260

261 **Author Information** The authors declare no competing financial interests.

262 Correspondence and requests for materials should be addressed to Z.S.S.
263 (she@pku.edu.cn).

264

265

266 **Figure Legends**

267 **Figure 1.** Validation of the multi-layer description of the mixing length profile and the
268 determination of the near-wall constants. Three sets of best resolved DNS data are used:
269 two channel flows from Iwamoto *et al.*²¹ at $Re_\tau \approx 650$ (black circles) and Hoyas and
270 Jimenez²² at $Re_\tau \approx 940$ (black squares), and one pipe flow of Wu and Moin²³
271 at $Re_\tau \approx 1142$ (blue triangles). (a): Compensated plot of the mixing length,
272 $\ell_M^{DNS} / (1 - r^m)$, illustrates four layers: sublayer, buffer, log-bulk and core. Two plateaus
273 ($m = 4$ for channel and $m = 5$ for pipe) illustrate the bulk flow structure, with the
274 same $\kappa = 0.45$. The solid lines are predictions of Eq.(1) using the measured κ and
275 other parameters. (b): Near-wall behaviour compared to theoretical prediction,
276 $\rho_0 / y_{sub}^{+3/2} \approx 0.0315$ (dashed line), finite- Re description of composite solution (solid
277 line), and corresponding buffer-layer description (dash-dotted line), which measure two
278 constants. The functions⁷ $B^{s-b} = (1 + (y^+ / y_{sub}^+)^4)^{1/8}$ and $B^{b-l} = (1 + (y^+ / y_{buf}^+)^4)^{-1/4}$.
279

280 **Figure 2.** Determination of the Karman constant, κ , and the core-layer thickness,
281 r_{core} . (a) Plot of measured $U_d^+(r) = U^+(0) - U^{+EXP}(r)$ versus theoretical function
282 $f(r, \bar{r}_{core})$, to illustrate a good linear relationship consistent with the measured universal
283 constant $\kappa \approx 0.45$, for both channel and pipe flows for a wide range of Re . Inset shows
284 the measurement for all Princeton data for $Re_\tau > 5000$. Star is the final measured value:
285 $r_{core}^{-EXP} \approx 0.67$ for Princeton data at relatively high Re , while $r_{core}^{-DNS} \approx 0.27$ for DNS data
286 at moderate Re , and $\kappa \approx 0.45$ in both cases. (b) Result of applying the procedure to

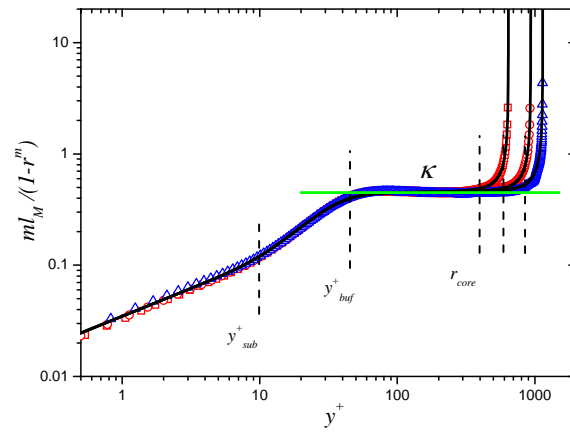
287 four sets of data: one theoretical profile generated from Eq.(1) and Eq.(2) to test the
 288 validity of the procedure, second profile with noise added to the former to test the
 289 robustness of the method, third profile from DNS channel simulation, and Princeton
 290 pipe data¹³. Note that the DNS profile follows closely the same error variation pattern as
 291 the theoretical profile, validating the theory with a clear determination of r_{core} and
 292 yielding a reliable estimate of κ and U_c^+ . On the other hand, the profile with small
 293 random noise (0.5%) yields an error variation pattern, closely resembling Princeton
 294 pipe data, which yields a scatter (20-30%) of the estimated r_{core} , but a much smaller
 295 uncertainty of κ (only 3%). This explains the scatter in the measured r_{core} presented
 296 in the inset of (a), and the slight variation of κ .

297

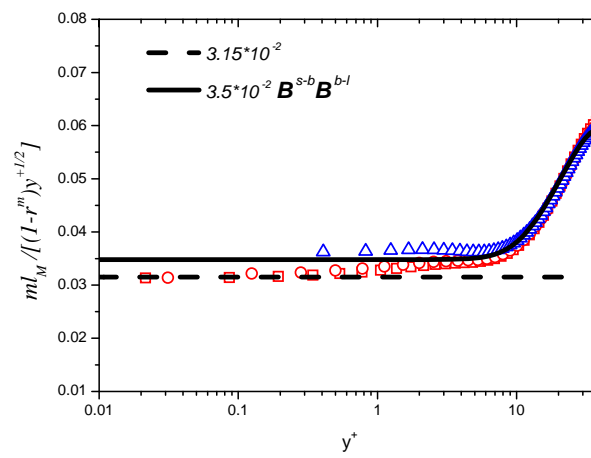
298 **Figure 3.** (a): Theoretical (solid lines) and measured MVPs, which are staggered
 299 vertically by five units for clarity. Inset shows the relative errors,
 300 $(U^{EXP} / U^{Theory} - 1) \times 100\%$. Note that errors in our theoretical predictions (red solid
 301 symbols) are uniformly within 1%. Also included is the recent model of L'vov,
 302 Proccacia and Rudenko (LPR¹⁹) (blue open symbols) - the only other theoretical model
 303 for entire MVP at finite Re . The LPR model has three adjustable parameters, the most
 304 important choices being $\kappa = 0.415$ for channel and 0.405 for pipe. It reveals
 305 systematic deviations at high Re . (b): Compensated plot of friction coefficient
 306 $C_f^{EXP} / C_f^{Pipe(\infty)}$ shows a transition around $Re_{\tau}^{(crit)} = 5000$ (black dot line). The dash line
 307 indicates $C_f^{EXP} = C_f^{Pipe(\infty)}$, and the dash-dot line is a linear finite Re model for both ε_{ρ}
 308 and ε_c given by Eq.(8) and (9). Inset compares the present prediction of

309 $(U_c^+ - \overline{U^+})^{Pipe} \approx 4.3$ (black dash line) to Princeton data (symbols), far improving previous
310 description in [3] (blue solid line).

311 **Figure 1.**



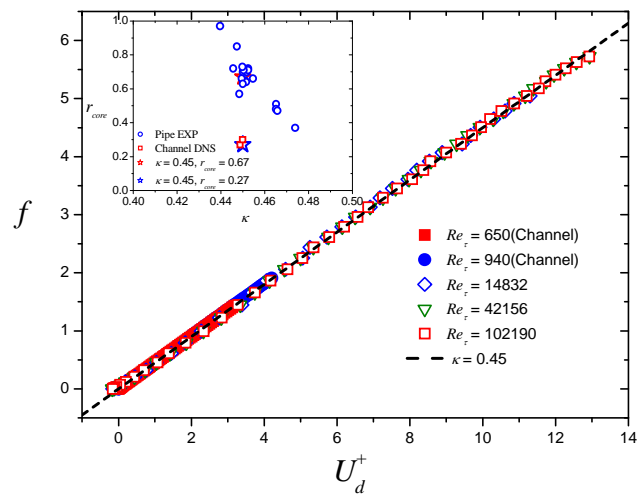
312



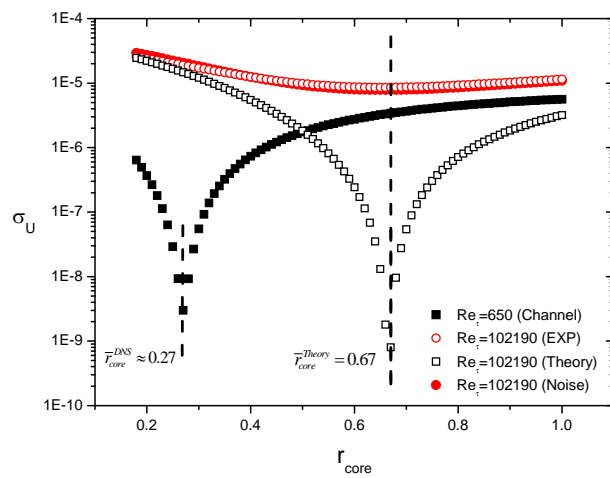
313

314

315 **Figure 2.**



316

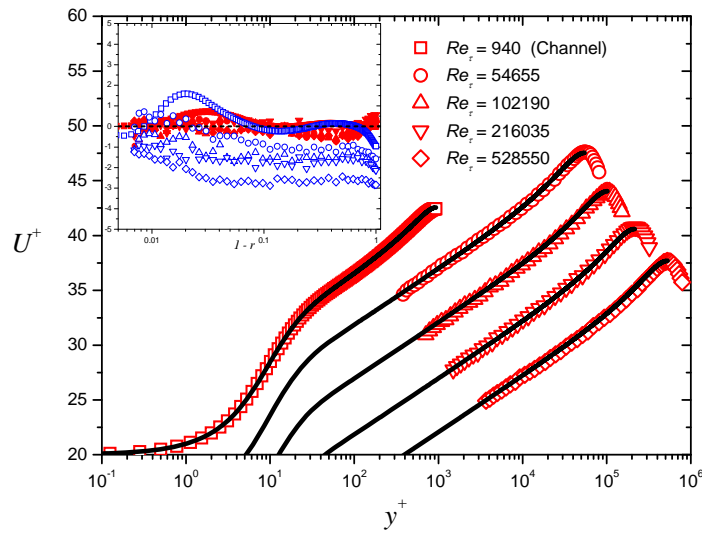


317

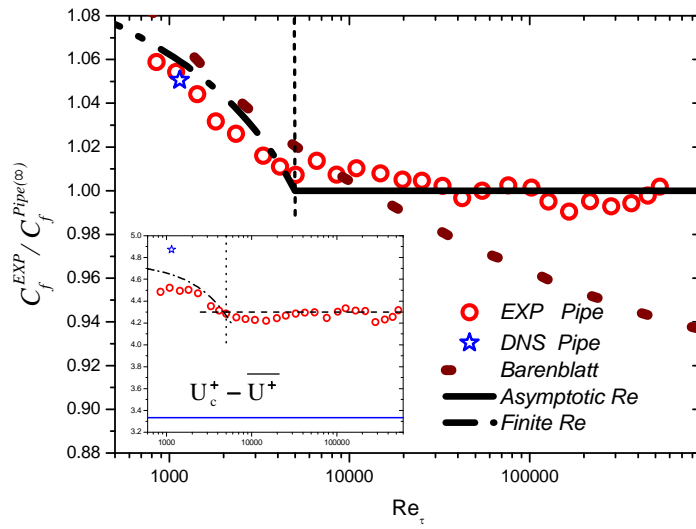
318

319

320 **Figure 3.**



321



322

323

324

325 **End**